



0191-8141(94)00112-X

## Rotation of fold-hinge lines associated with simple shear during southerly directed thrusting, Ouachita Mountains, southeastern Oklahoma

QINGMING YANG and KENT C. NIELSEN

Programs in Geosciences, The University of Texas at Dallas, P.O. Box 830688, Richardson, TX 75083, U.S.A.

(Received 1 July 1993; accepted in revised form 29 September 1994)

**Abstract**—The Broken Bow uplift in southeastern Oklahoma contains the oldest rocks exposed in Ouachita orogenic belts and has experienced four phases of deformation. First-generation folds are tight, overturned, S-verging, and have a well developed slaty cleavage. Second-generation folds are coaxial with first-generation structures, are open to tight, are inclined, and reveal S-vergence. Northerly dipping faults truncate second-generation fold limbs. Third-phase structures, including recumbent folds and pencil structures, are interpreted to be contemporaneous with S-directed thrusting. The hinges of earlier folds documented in the area least affected by thrusting are horizontal and trend E–W. The hinges of folds of the same generation within fault zones plunge 30–50° toward the north or northwest. Thus, it is concluded that the earlier folds have been passively rotated during S-directed thrusting, as have the contemporaneous folds and pencil structures. A simple-shear model associated with S-directed thrusting is proposed to explain these geometrical relations. The rotated fold hinges provide quantifiable shear-strain gauges which can be used to quantify shear strain in the Broken Bow uplift as well as in other orogenic belts. A model for shear-strain calculation is developed using the general geometric relationship between fold-hinge lines, the shear direction, and the shear plane.

### INTRODUCTION

Subparallelism of fold-hinge lines and stretching lineations, such as deformed pebbles, pressure shadows, and feldspar has been reported in many orogenic belts (e.g. Bryant & Reed 1969, Borradaile 1972, Roberts & Sanderson 1973, Bell 1978, Quinquis *et al.* 1978, Alsop 1992). Stretching lineations often parallel the tectonic transport or shear direction of deformation in high-shear-strain zones. The alignment of fold-hinge lines and stretching lineations is therefore believed to result from passive rotation of fold-hinge lines towards the shear direction during progressive deformation (Bryant & Reed 1969, Roberts & Sanderson 1973, Escher & Watterson 1974, Bell 1978, Williams 1978, Alsop 1992). Fold-hinge lines are rotated into parallelism with this direction either because small initial irregularities have become amplified in progressive strain (Cobbold & Quinquis 1980), or because the strain field includes a wrench shear component developed where there is a gradient in the shear strain rate in a direction perpendicular to the slip direction (Coward & Potts 1983, Ridley 1986). The tectonic setting of this type of deformation has most commonly been studied in highly deformed mid-crustal regions of orogenic belts (Borradaile 1972, Roberts & Sanderson 1973, Rhodes & Gayer 1977, Bell 1978, Williams 1978, Alsop 1992).

By examining the geometry of sheath folds in the Monte Rosa Nappe, Swiss Alps, Lacassin & Mattauer (1985) were able to calculate the shear strain associated with passive rotation of sheath-fold-hinge lines. Although this model makes a number of assumptions, it provides a gross estimate of regional shear strain variation, especially where traditional strain markers are

lacking. Using Lacassin & Mattauer's model (1985), Alsop (1992) evaluated the shear strain associated with rotation of folds involved in crustal scale thrusting in lower amphibolite-facies metasedimentary rocks of northwest Ireland. Alsop (1992) demonstrated that fold rotation is associated with temporal and spatial evolution of the Ballybofey Nappe.

This article presents a detailed study of structures in the Broken Bow uplift of the Ouachita Mountains in southeast Oklahoma, where deformation and rotation of fold-hinge lines is believed to have occurred in the upper crust. A model for shear-strain calculation is developed using the general geometric relationship between fold-hinge lines, the shear direction, and the shear plane. This relationship represents a generalization on an existing model by Alsop (1992) and provides insight into geometric and kinematic characteristics of thrust nappe emplacement.

### GEOLOGICAL SETTING

The Ouachita Mountains consist of folded Paleozoic rocks that trend westward across Arkansas into Oklahoma from beneath Mesozoic–Tertiary strata of the Gulf Coastal Plain (Viele 1989) (Fig. 1). In Oklahoma this belt turns southwestward and disappears beneath Mesozoic–Tertiary cover rocks. The Marathon uplift of southwest Texas and Ouachita Mountains of southeast Oklahoma and west-central Arkansas are the only surface exposures of the deformed belt.

The Ouachita Mountains were deformed during Middle Pennsylvanian–Early Permian time. Deformation is generally believed to be due to a collision between North

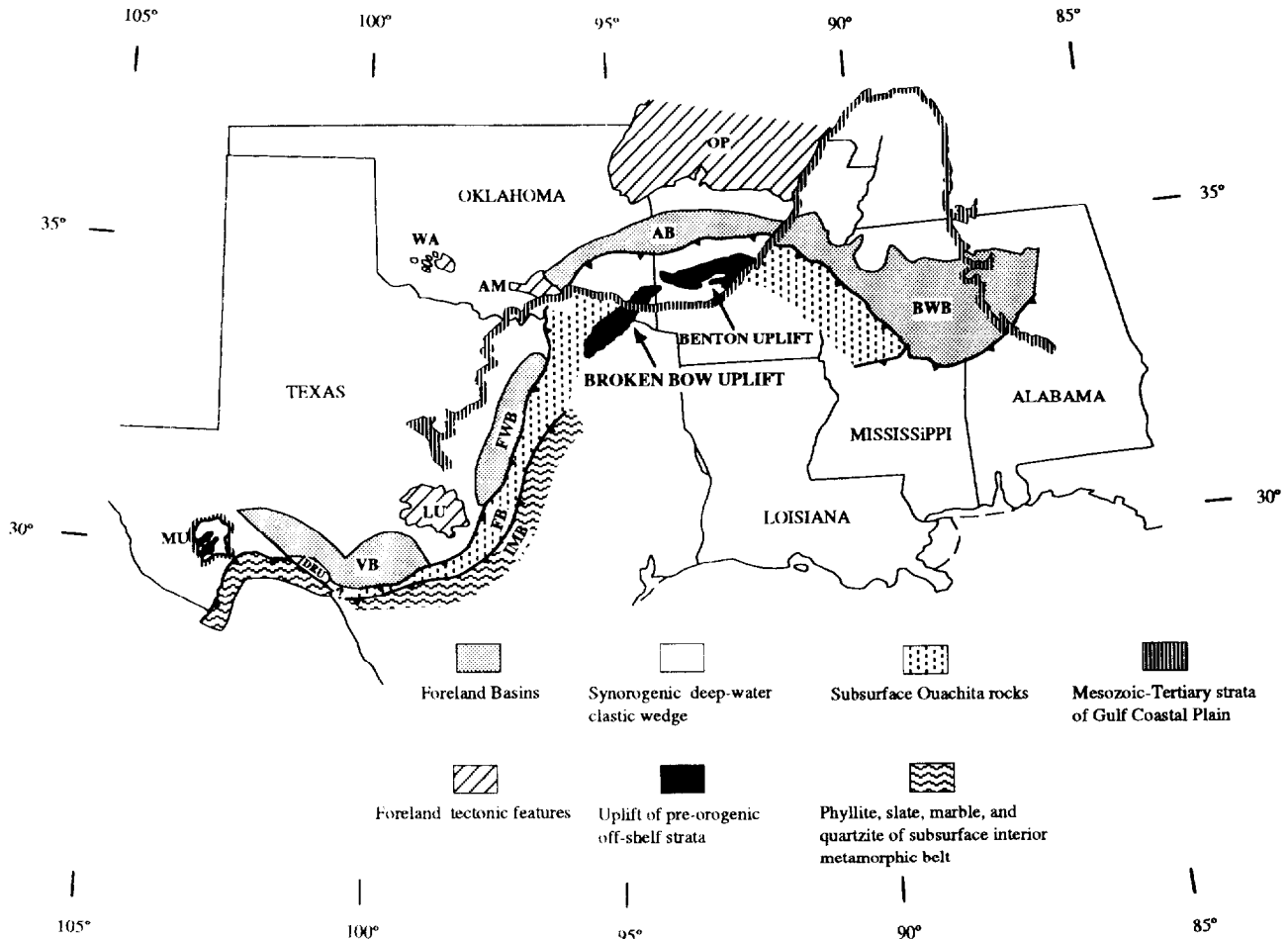


Fig. 1. Index map of the Ouachita System across southern North America (after Viele 1989). AB = Arkoma basin, AM = Arbuckle Mountain, BWB = Black Warrior basin, DRU = Devils River Uplift, FB = Frontal belt, FWB = Fort Worth basin, IMB = Interior metamorphic belt, LU = Llano uplift, MU = Marathon uplift, OP = Ozark plateau, VB = Val Verde-Kerr basin. WA = Wichita Mountain.

America and an unknown continent or accreted terrane and island arc (Mickus & Keller 1992). Ham & Wilson (1967) believed that deformation in the Ouachitas were diachronous and that it took place during Middle Pennsylvanian time in Oklahoma and Arkansas and during Late Pennsylvanian through Early Permian time in the Marathon region. Denison *et al.* (1969) argued that orogeny in the Ouachita Mountains was most intense during Late Pennsylvanian time.

Rocks in the Broken Bow uplift are characterized by low-grade metamorphic assemblages. Although regional metamorphism may have reached lower greenschist facies, rocks in the Broken Bow uplift are generally of zeolite facies (Flawn *et al.* 1961, Denison *et al.* 1977). In the southern portion of the Broken Bow uplift, shale units such as the Womble Formation (Fig. 2) have been metamorphosed to low-grade slate or phyllite (Denison *et al.* 1977). Studies using fluid inclusions from quartz and other vein minerals indicate that temperatures ranged from 100°C to 315°C (Houseknecht & Matthews 1985, Keller *et al.* 1985). Herrin & Clark (1956) studied heat flow in west Texas and eastern New Mexico and concluded that the temperature gradient in interbedded sand and shale sequences is about 20°C km<sup>-1</sup>. Adapting this geothermal gradient, the depth of metamorphism and presumably that of deforma-

tion in the Ouachita Mountains ranged from 5 to approximately 16 km, i.e. the upper crust.

Feenstra & Wickham (1975) divided the Oklahoma portion of the Ouachita Mountain into three structural provinces. The frontal province is a highly imbricated thrust zone bounded to the north by the Choctaw fault and to the south by the Windingstair fault. The frontal province varies in width from 2.4 km in the west to 19 km in the east and consists of many narrowly-spaced, N-verging thrust slices (Arbenz 1989). The central province is bounded on the north by the Windingstair fault and on the south by the Broken Bow uplift and is characterized by a few large synclines cut by reverse faults. The core province refers to the older more complexly deformed rocks exposed in the Broken Bow uplift.

Rocks in the Broken Bow uplift range in age from Late Cambrian–Mississippian. These sedimentary rocks include dark shales, cherts and sandstones, and are characterized by a series of S-verging asymmetrical folds which are cut by N-dipping faults. Nielsen (1985) and Nielsen *et al.* (1989) subdivided the Broken Bow uplift into four large structures (Fig. 3). To the north, the Cross Mountain anticlinorium is a large, doubly-plunging structure approximately 50 km long along strike. The Linson Creek synclinorium, which lies to the

AGE	GROUP OR FORMATION	DESCRIPTION
MISSISSIPPIAN	STANLEY (1800-3600 meters)	Shales with interbedded siltstone and fine grained sandstone. Tuff beds near the base. Cleavages well developed in shales and siltstones.
	ARKANSAS NOVACULITE (90 meters)	Thick bedded white cherts in the lower member. Middle member shale with interbedded chert. Upper member thick bedded dark chert with interbedded shale.
DEVONIAN		
SILURIAN	BLAYLOCK (270-300 meters)	Missouri Mountain red and green shales with interbedded sandstone, soft sediment deformation.  Blaylock massive thin to medium bedded siltstone and dark shale. Graded bedding, sole marks, well developed slaty cleavage, and mesoscopic folds.  Polk Creek shale at the bottom.
ORDOVICIAN	BIGFORK (120-240 meters)	Bigfork massive thick bedded cherts and interbedded shales.
	WOMBLE (150 meters)	Shales and slates with schistose sandstone and conglomerate.

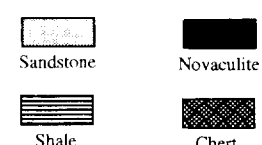


Fig. 2. Simplified stratigraphic column for the flank sequence of the Broken Bow uplift, southeastern Oklahoma (modified from Honess 1923, Feenstra & Wickham 1975). Missouri Mountain shale and Polk Creek shale are mapped as part of the Blaylock Formation.

south of the Cross Mountain anticlinorium, is dominated by exposures of the lower Stanley Shale, although three doubly plunging, nearly upright folds of the Arkansas Novaculite crop out in the trough of the synclinorium. The Carter Mountain anticlinorium is the next structure to the south. The Hochatown dome is separated from the Carter Mountain anticlinorium by the Dyer Mountain fault zone (Fig. 3). This study focuses in the western portion of Carter Mountain anticlinorium and the Dyer Mountain fault zone (Fig. 4).

#### FOLD GEOMETRY AND SEQUENTIAL DEFORMATION OF THE FOOTWALL OF DYER MOUNTAIN FAULT ZONE

The western flank of the Carter Mountain anticlinorium and the Dyer Mountain fault zone (DMFZ) is

characterized by a multiply deformed middle Paleozoic sequence (Honess 1923, Feenstra & Wickham 1975) (Fig. 2). Analysis of macroscopic and mesoscopic structures in the footwall of the DMFZ indicates a complex, polyphase deformational history with at least four phases of deformation (Nielsen & Yang 1992). First-generation folds are tight to isoclinal, asymmetric, overturned to the south, subhorizontal with planar limbs and sharp hinges that trend E-W (Fig. 5). First-generation folds have been significantly modified during folding associated with later deformation and the axial surfaces are curvilinear. Upright limbs are attenuated and overturned limbs are thickened, similar to those seen by Mies (1991). Regionally developed slaty cleavage is associated with the earliest folds and is most common in the southern half of the Broken Bow uplift. We have previously argued that pressure solution is the dominant mechanism of the cleavage formation (Yang & Nielsen 1992b).

Second-generation folds are coaxial with first-generation structures, but are open to tight, inclined, and S-verging. These folds have curved limbs with subhorizontal curved hinges that trend east-west (Fig. 6). Second-generation folds are identified based on the folded earlier slaty cleavage (Mattes & Nielsen 1983, Nielsen 1985, Nielsen *et al.* 1989, Yang & Nielsen 1992b). On the south limb of the synform, cleavage dips to the north, and on the north limb of the synform, the cleavage dips to the south (Yang & Nielsen 1992b). A megascopic second-generation synform has been mapped just south of the DMFZ (Fig. 4). Slaty cleavage associated with this S-verging syncline dips to the south on the north limb, also indicating folding of the earlier slaty cleavage.

A series of N-dipping faults truncate first- and second-generation folds. Northerly dipping faults appear to have rotated the earlier fold-hinge lines. Third-phase structures include recumbent folds developed in the steeply dipping limbs of first- and second-generation folds (Fig. 7), pencil structures, and a locally developed spaced cleavage. These are interpreted to be related to flattening as a result of tectonic thickening associated with S-directed thrusting. Fourth-phase structures include crenulation cleavage and a family of open and upright NE-trending folds. Although deformation has been divided into four phases based on geometry, style, refolding and truncating relations, the deformation is believed to have been progressive and represents a tectonic continuum during late Carboniferous rather than a series of events separated in time (Nielsen *et al.* 1989, Yang & Nielsen 1992b). This is particularly true for the first-, second- and third-generation structures.

#### DYER MOUNTAIN FAULT ZONE

The Dyer Mountain fault zone separates the northwest portion of the Hochatown dome and Carter Mountain anticlinorium (Nielsen *et al.* 1989, Yang & Nielsen 1992a, Nielsen & Yang in press) (Fig. 4). The DMFZ

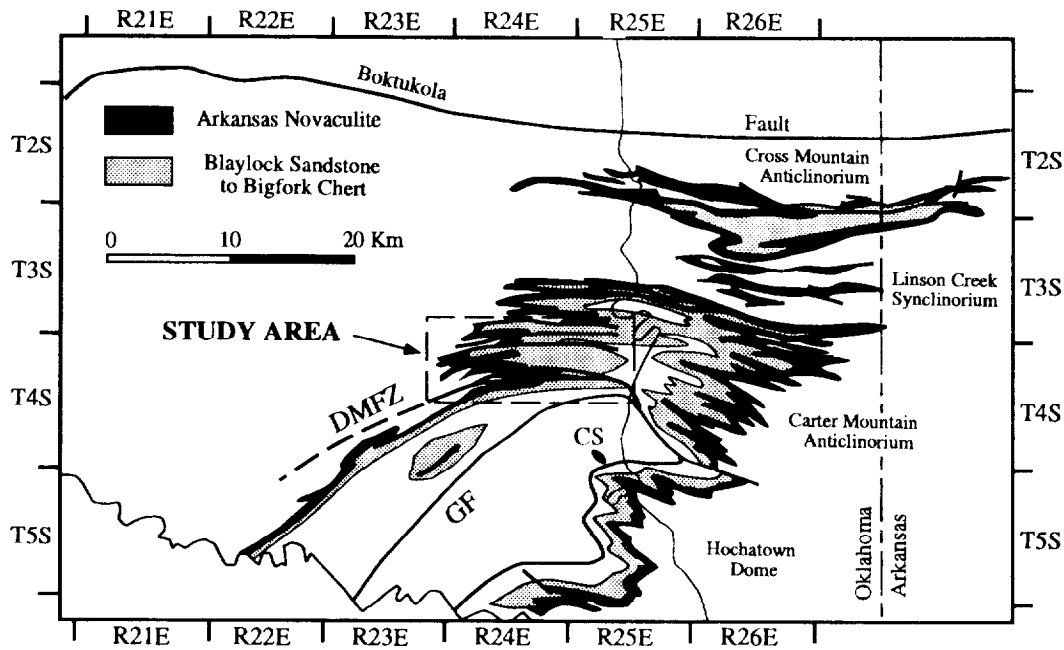


Fig. 3. Subdivisions of the Broken Bow uplift (after Nielsen *et al.* 1989) and location of study area and deformed clasts (CS). DMFZ = Dyer Mountain fault zone. The Glover fault (GF) is interpreted to be related to formation of the uplift and is younger than the DMFZ.

can be followed from the Stanley Formation on the western flank to the Broken Bow reservoir (10 km) (Fig. 4). Within the fault zone, slices of Arkansas Novaculite and tightened fold hinges have been isolated by the faults. At the Broken Bow reservoir, the Bigfork Chert is in fault contact with upright Blaylock Sandstone (Fig. 4). While stratigraphic units along DMFZ near the lake shore indicate reverse separation, a cross-section across the fault zone west of the culmination in the anticlinorium (A–A' in Fig. 8) shows normal separation. Striations and small steps identified on the slickensides in the DMFZ indicate normal motion within the DMFZ (Yang 1993). Honess (1923) concluded that many of these N-dipping faults are normal faults associated with uplift. Viele & Thomas (1989) suggested that these faults were originally N-directed thrust faults that were rotated during later folding resulting in normal separation.

The history of the DMFZ includes initial formation as a thrust and reactivation as a normal fault during later stages of deformation. Mesoscopic structures near the DMFZ indicate that the S-verging second-generation structures are associated with the initial thrust motion in the DMFZ. Therefore, the earliest folds predate the DMFZ while the second-generation folds are directly related to its development. A common feature of the second-generation folds is truncation of the north limb of second-generation synclines by a N-dipping fault. These faults appear to repeat the section in the upright limbs of first-generation folds, and cause zones of disrupted folds in the overturned limbs of first-generation folds (Nielsen & Yang *in press*).

While the hinges of the first- and second-generation folds in the N-flank of Hochatown dome are subhorizontal and trend E–W, hinges of folds of the same generation within Dyer Mountain, South Carter Creek, and North Bee Creek fault zones plunge 30–55° to the north

and northwest (Yang & Nielsen 1993) (Fig. 9). As the DMFZ is approached from the south, the folds plunge progressively steeper, 15–20°, toward the west-northwest. This variation in orientation is interpreted to reflect rotation associated with fault movement and will be discussed in detail in following sections. Deformed shale clasts within the Womble Formation are found in the footwall of the DMFZ along the eastern flank of the Hochatown dome. The clasts vary in size from less than 1 cm to as large as 45 cm in the elongated dimension. The composition of these clasts varies from shale to fine grained siltstone and it is very similar to that of the matrix, suggesting an origin as an intraformational debris flow with little competency contrast during subsequent deformation. Long axes of these deformed clasts plunge less than 25° NW or SE, with the most commonly observed azimuth of 326° or 146° (Fig. 10). A Flinn plot (Flinn 1962) indicates that most of the clasts fall in the field of apparent constrictional strain (Fig. 11a). In addition, a high symmetry-index value of 0.93 calculated using  $R_1/\phi$  plot suggests that the clasts lack an initial preferred orientation (Lisle 1985) (Fig. 11b). Clearly, a wide range of strain paths are possible for these clasts, but the strong preferred orientation suggests a dominant elongation direction in close proximity to the overlying faults. This extension direction is interpreted to approximate the tectonic transport direction or shear direction in high-shear-strain zones (Lacassin & Mattauer 1985).

#### CARTER MOUNTAIN ANTICLINORIUM

The southwestern portion of the Carter Mountain anticlinorium has been subdivided into anticlines

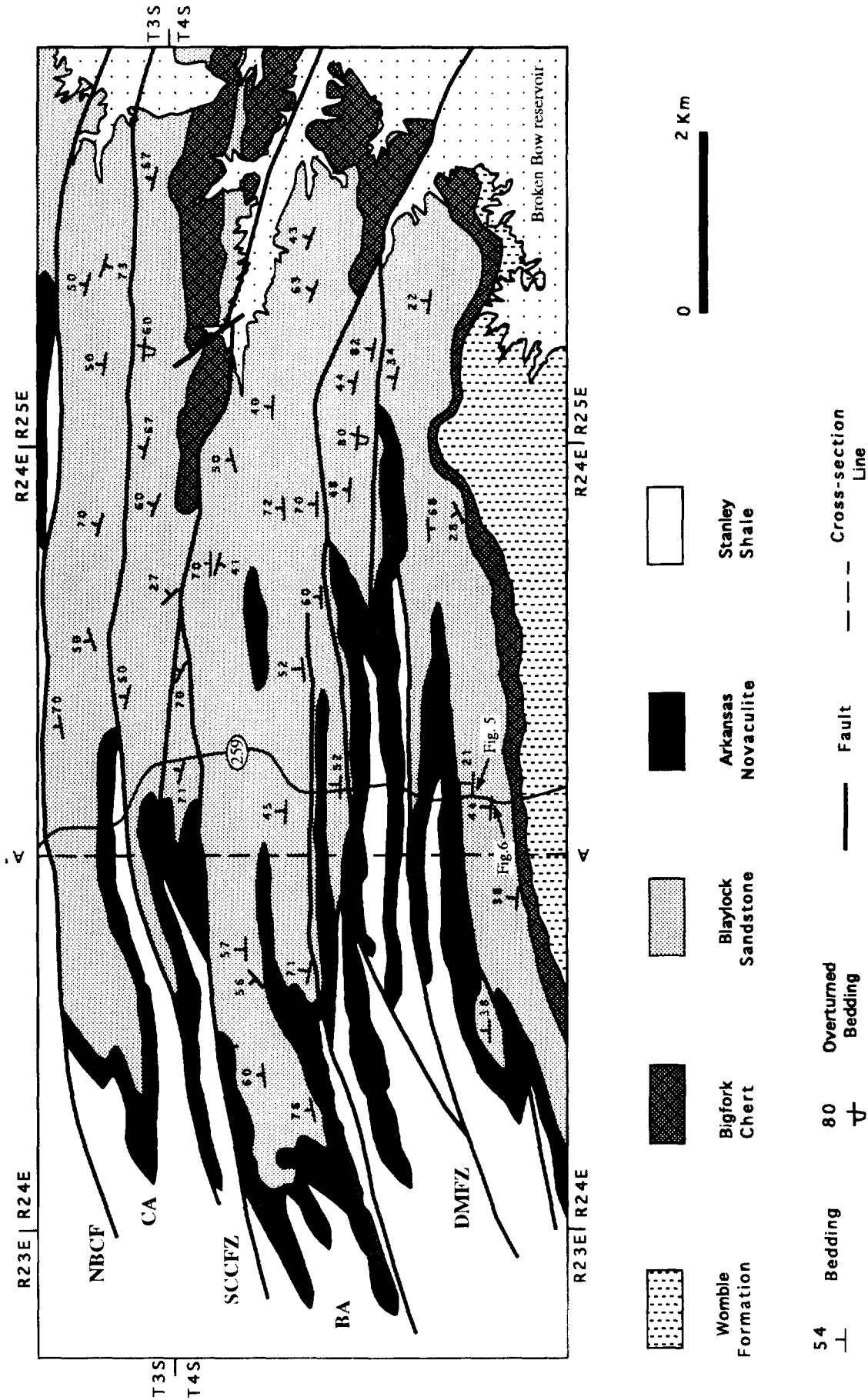


Fig. 4. Geological map of the study area on the western flank of the Carter Mountain anticlinorium. The broadly spaced dot pattern is the Broken Bow reservoir. Highway 259 is the irregular line trending N-S just east of the cross-section line A-A'. DMFZ = Dyer Mountain fault zone, BA = Brigham anticline, SCCFZ = South Carter Creek fault zone, CA = Carter Mountain anticline, NBCF = North Bee Creek fault.

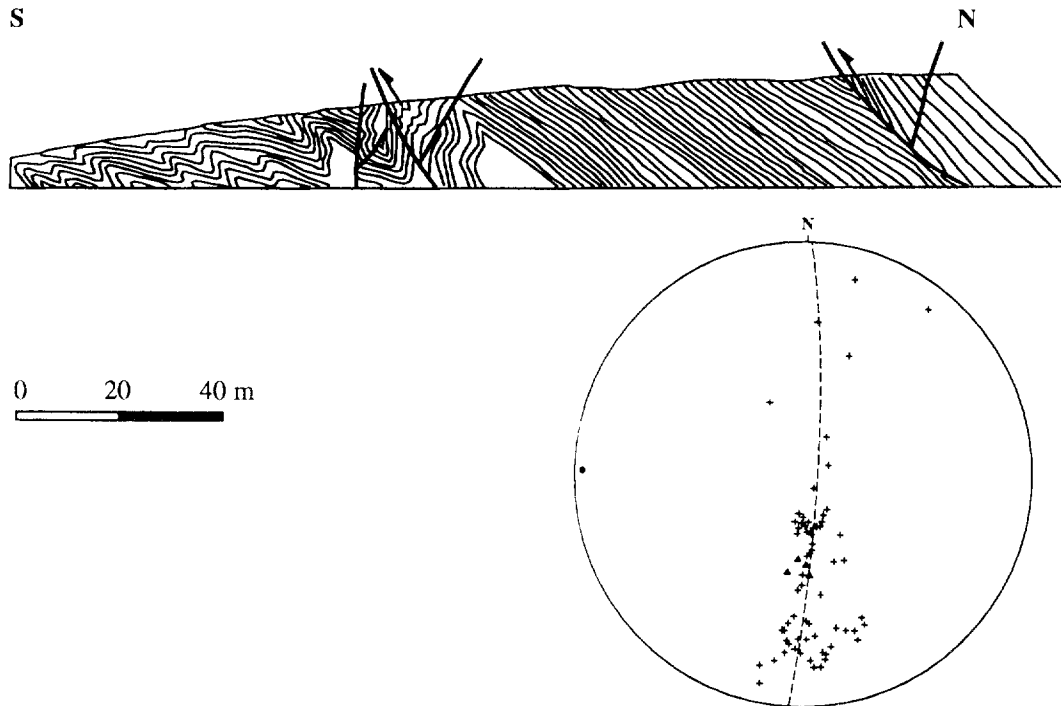


Fig. 5. Outcrop sketch and lower-hemisphere equal-area projections of orientation data of first-generation folds of Blaylock Sandstone in the footwall of the DMFZ, along highway 259. Poles to bedding are crosses ( $n = 69$ ), poles to cleavages are triangles ( $n = 4$ ), and cylindrical best-fit fold axis ( $270^{\circ}/74^{\circ}$ ) (bearing/plunge) is the dot. Mean dips for bedding in the upright limb and overturned limb are  $82^{\circ}/25^{\circ}\text{N}$  (strike/dip) and  $88^{\circ}/68^{\circ}\text{N}$ , respectively; the mean dip of cleavage is  $90^{\circ}/41^{\circ}\text{N}$ .

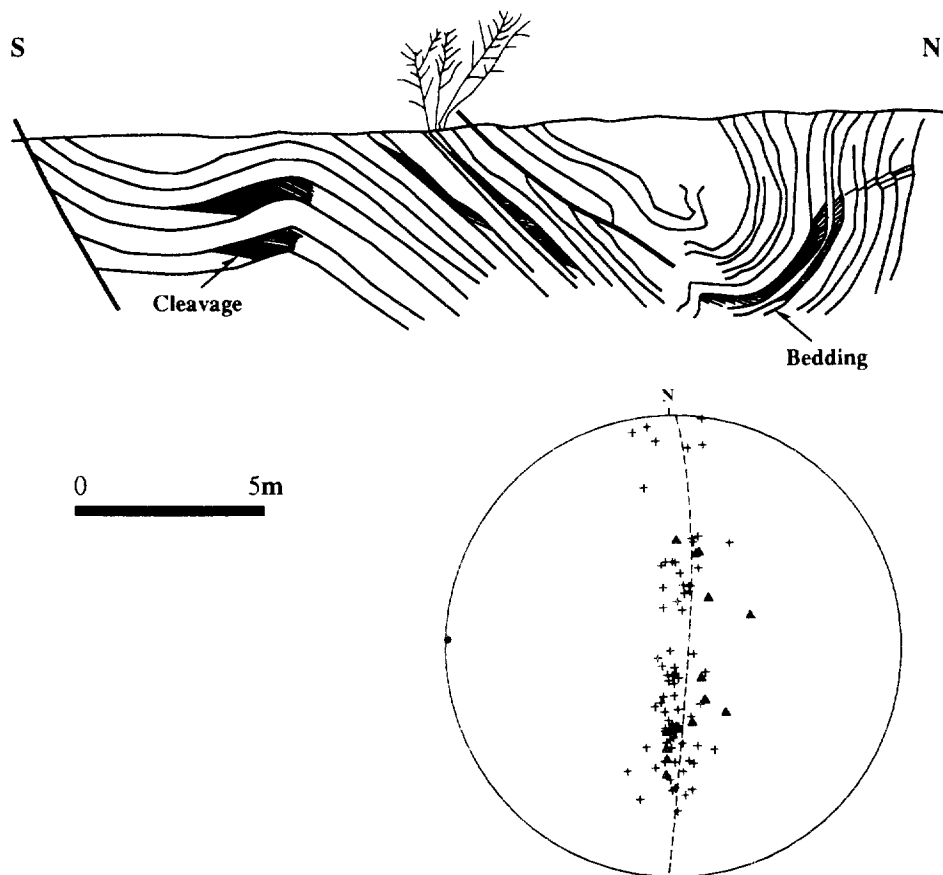


Fig. 6. Outcrop sketch and lower-hemisphere equal-area projections of orientation data of a second-generation syncline characterized by folded slaty cleavage. Note a small first-generation anticline located in the hinge of the larger second-generation syncline. Closely spaced dark lines in the sketch represent slaty cleavages; heavy lines are faults. Three second-generation mesoscopic folds near this outcrop were identified. The projection includes data from all the three of these folds. Poles to bedding are crosses ( $n = 79$ ), poles to cleavage are triangles ( $n = 15$ ), and cylindrical best-fit fold axis is the dot ( $273^{\circ}/1^{\circ}$ ). The southern limb of the second-generation syncline dips  $92^{\circ}/28^{\circ}\text{N}$  and the northern limb dips  $90^{\circ}/80^{\circ}\text{S}$ .

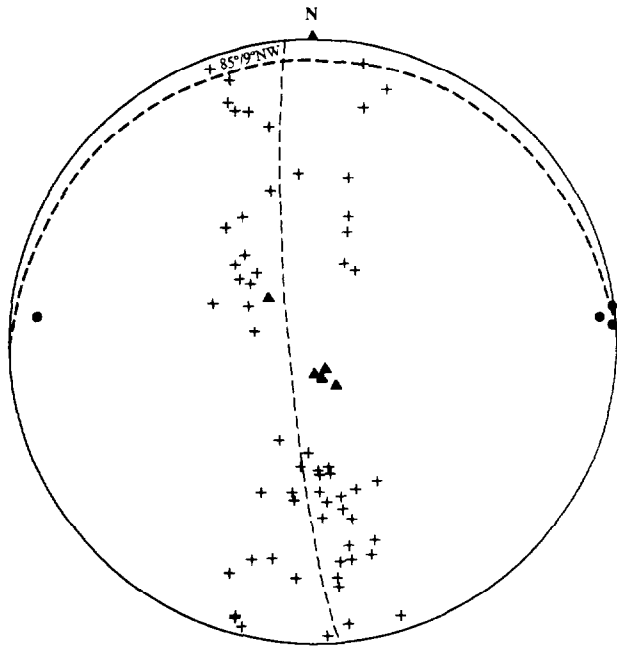


Fig. 7. Lower-hemisphere equal-area projections of data from recumbent folds associated with the third-generation of deformation. Poles to bedding are crosses ( $n = 61$ ), pole to axial plane cleavage ( $85^{\circ}/9^{\circ}$ NW) are triangles ( $n = 5$ ), fold-hinge lines ( $85^{\circ}/0^{\circ}$ ) are dots ( $n = 4$ ), the N-dipping limb is  $87^{\circ}/54^{\circ}$ NW and the S-dipping limb is  $82^{\circ}/47^{\circ}$ SE.

separated by fault zones. Successive structures, from south to north, are described in the following sections (Fig. 4).

*Brigham anticline*

The Brigham anticline consists of two smaller parasitic anticlines with one syncline in the center (Figs. 4

and 8). These folds are outlined by outcrop of the Arkansas Novaculite along the western flank of the uplift. The Blaylock Sandstone crops out over most of the area. The Bigfork Chert is exposed in the east, near the lake shore. These folds are cylindrical, asymmetric, overturned to the south and are characterized by planar limbs with interlimb angles of  $40\text{--}60^{\circ}$  and sharp hinges that plunge slightly (less than  $10^{\circ}$ ) to the west (Fig. 8). Slaty cleavage is subparallel to the axial surface. Based on the characteristics of the hinge, interlimb angle, cleavage and orientation, Brigham anticline is interpreted as due to the earliest deformation.

*South Carter Creek fault zone*

The South Carter Creek fault zone (SCCFZ) separates the Carter Mountain anticline to the north and the Brigham anticline to the south (Figs. 4 and 8). Two boundary faults have been identified, within this fault zone, surrounding a horse of a folded thick sequence of Arkansas Novaculite. Field data indicate that the hinge line of the folded Arkansas Novaculite has a bearing and plunge of  $350^{\circ}/45^{\circ}$  (Figs. 4 and 9). Mesoscopic folds of an earlier generation developed in the Blaylock Sandstone within this horse also plunge moderately to the northwest and north. In addition, 'recumbent folds', interpreted as third-generation structures, are found at this location and are believed to have resulted from flattening during S-directed thrusting. These folds are cylindrical with interlimb angles of approximately  $90^{\circ}$ , have relatively planar limbs and sharp hinges that plunge  $35\text{--}40^{\circ}$ NW.

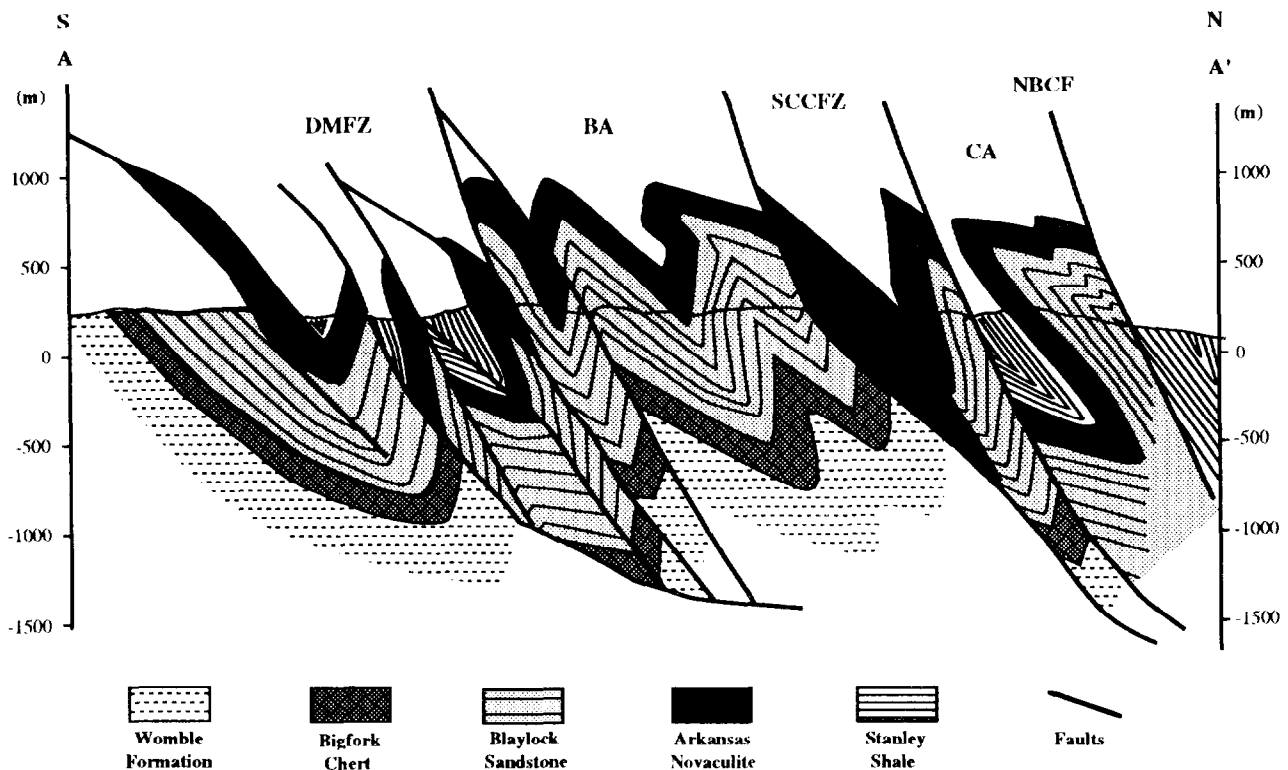


Fig. 8. A down-plunge view of the western flank of the Carter Mountain anticlinorium, the DMFZ, and the footwall of DMFZ. No vertical exaggeration.

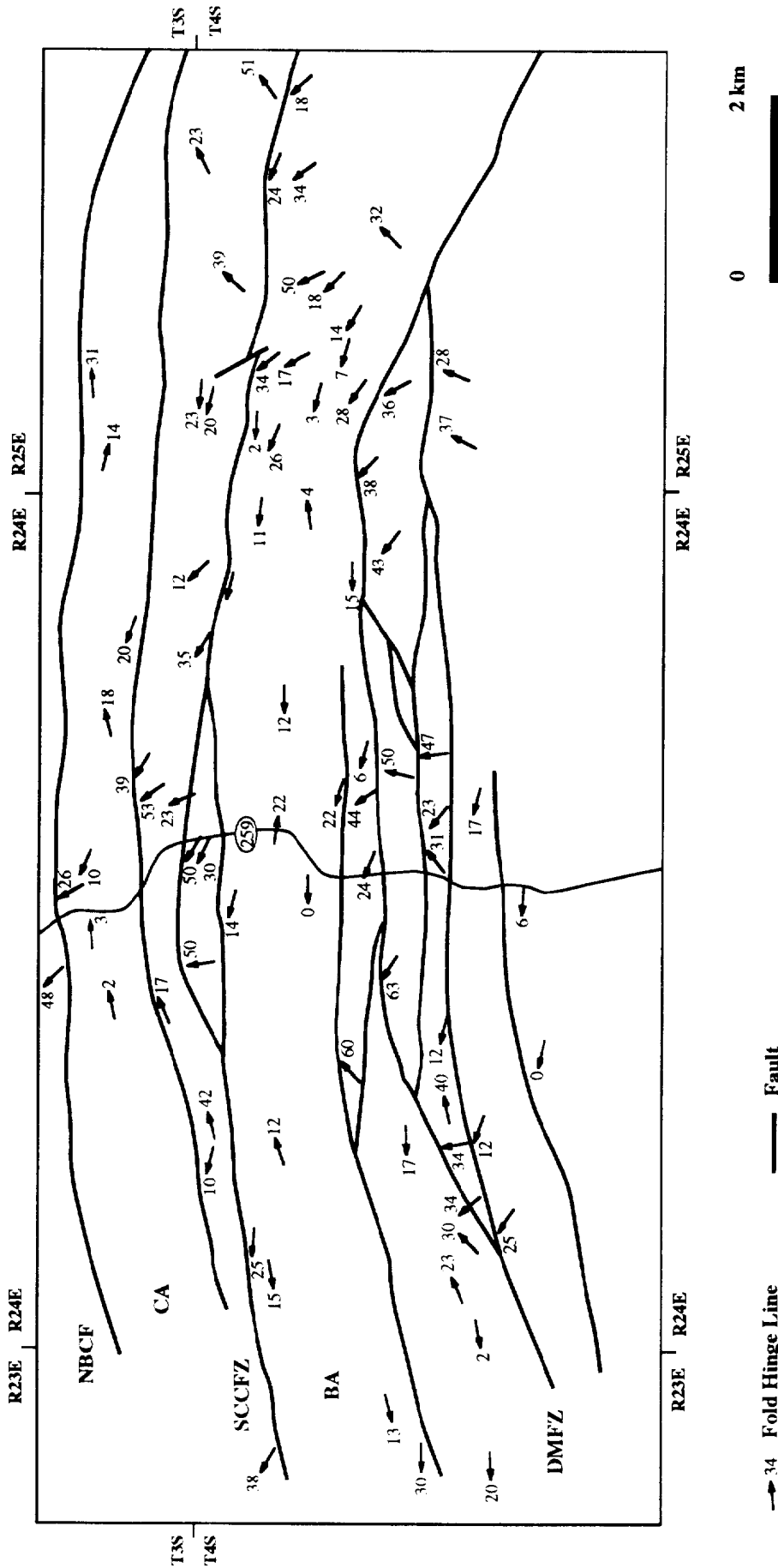


Fig. 9. Distribution of first- and second-generation fold-hinge lines across the study area. The heavy lines are fault traces. Highway 259 is the irregular line trending N-S. Arrows represent fold-hinge lines and numbers are plunge angles. Folds of fold-hinge lines represent the sample locations.



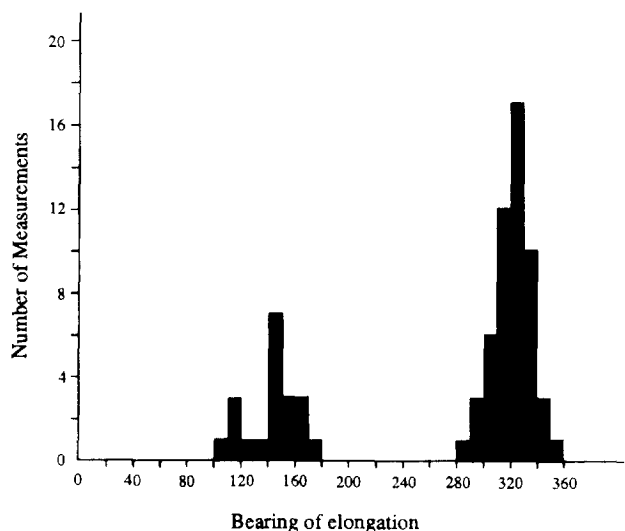


Fig. 10. The bearing of principal elongation axes of deformed clasts in the Womble Formation directly below the DMFZ ( $n = 73$ ).

*Carter Mountain anticline*

The Carter Mountain anticline is an E-W-trending anticline with a parasitic anticline and syncline developed on its northern limb (Fig. 4). The Carter Mountain anticline has relatively planar limbs, a sharp hinge and has interlimb angles of 40–50°. The fold is cylindrical, asymmetric, and is overturned to the south. The Carter Mountain anticline is interpreted to be equivalent to the

earliest folds described in the footwall of the DMFZ. The slaty cleavage is axial planar to the Carter Mountain anticline. This fold is truncated to the north by North Bee Creek fault zone (NBCF) and to the south by SCCFZ (Fig. 4).

*North Bee Creek fault zone*

On the north side of Carter Mountain, the North Bee Creek fault zone (NBCF) truncates the Carter Mountain anticline and juxtaposes the Mississippian Stanley Formation against the Silurian Blaylock Formation (Hones 1923) (Fig. 4). This fault zone is thought to have a history comparable to the DMFZ.

**SIGNIFICANCE OF FOLD-HINGE LINE DISTRIBUTION**

Geological data suggest that the pre-existing and contemporaneous folds within fault zones of the Broken Bow uplift have been passively rotated towards the extension direction during S-directed thrusting. The earlier folds in the footwall of the DMFZ, the Brigham anticline, and the Carter Mountain anticline trend E-W and show no rotation (Fig. 9). The recumbent folds developed on the steeply dipping limbs of earlier structures are interpreted to be contemporaneous folds (Sanderson 1973, Williams 1978). These recumbent folds and

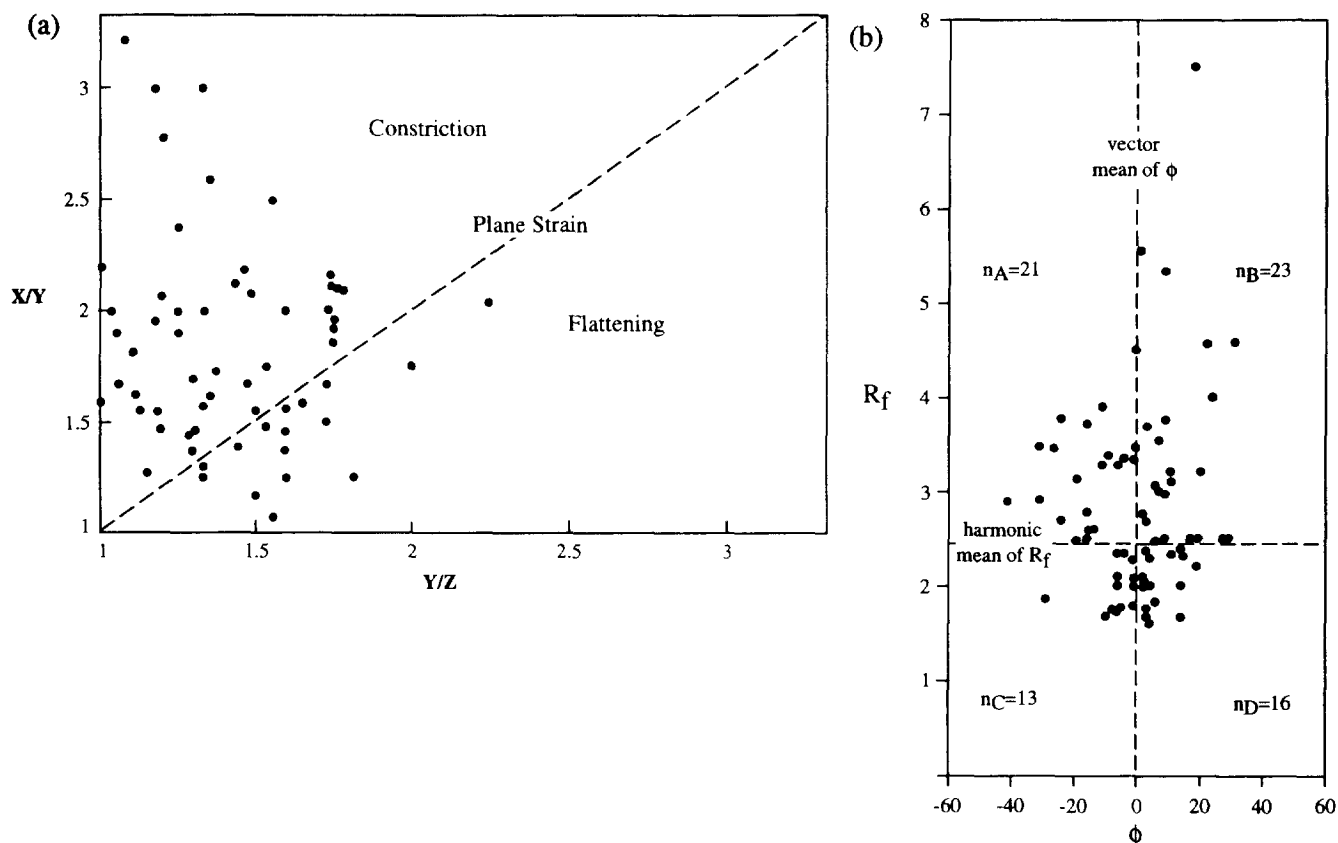


Fig. 11. (a) Flinn plot showing aspect ratios of deformed clasts in Womble Formation below the DMFZ along the eastern flank (see Fig. 2).  $X$ ,  $Y$  and  $Z$  represent long, intermediate and short axes of deformed clasts, respectively. (b)  $R_f/\phi$  plot of the same data set shown in Fig. 11(a).  $n_A$ ,  $n_B$ ,  $n_C$  and  $n_D$  represent number of deformed clasts within each respective quadrant.  $R_f$  represents the aspect ratio of long axes and short axes of deformed clasts.

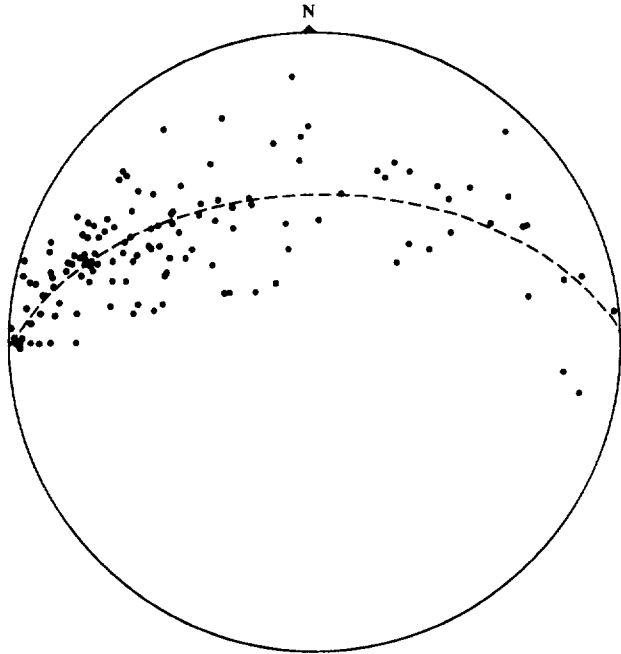


Fig. 12. Lower-hemisphere equal-area projections of all fold-hinge lines measured in the study area ( $n = 135$ ). The best fit great circle approximates the attitude of the shear plane ( $88^{\circ}/51^{\circ}\text{N}$ ).

coeval pencil structures are believed to be products of regional flattening associated with southerly directed thrusting (Nielsen & Yang 1992). These structures also appear to have been rotated.

Rotation of fold-hinge lines in the study area cannot be explained by refolding because: (1) second- and third-generation deformations are coaxial with the first; and (2) the hinge lines of earlier and contemporaneous folds are rotated only within the fault zones or near the fault zones. All the hinge lines including first-, second- and third-generation folds in the footwall of the DMFZ, Brigham anticline and Carter Mountain anticline are trending E–W and do not show rotation.

Rotation of fold-hinge lines toward the extension direction can be accomplished in a variety of ways. Borradaile (1972) showed that rotation of fold-hinge lines can be achieved by progressive, irrotational, constrictional deformation. Sanderson (1973) and Ramsay (1979) suggested that this rotation can also be accomplished by flattening. Escher & Watterson (1974), Williams (1978), Minnigh (1979) among others have demonstrated that pre-existing folds or contemporary folds can be passively rotated toward the X-direction as a result of simple shear associated with thrusting. By any account, the amount of rotation depends on the orientation of initial fold-hinge lines and the magnitude and type of strain.

Although rotation of fold-hinge lines at upper crustal levels has been documented in other orogenic belts (e.g. Wojtal 1986, Handschy 1989, Cowan & Brandon 1994), only Handschy's work compares with ours in the size of the rock mass where fold-hinge lines are affected by fault-related shear. Fold-hinge lines from the study area are dispersed in a N-dipping plane. The best fit great

circle for the rotated fold-hinge lines data has a strike and dip of  $88^{\circ}/51^{\circ}\text{N}$  (Fig. 12).

Deformation due to simple shear exists not only in the Broken Bow uplift but in the Benton uplift as well (Fig. 1). Sturges (1986) studied the Alum Fork area of the Benton uplift in Arkansas. He found that hinge lines of  $F_2$  folds are curvilinear and define a continuous great circle, approximately parallel to the average axial plane of the  $F_2$  phase folding. He observed that stretching lineations on many cleavage surfaces throughout the area coincide with the maximum concentration of  $F_2$  hinge lines. Sturges (1986) demonstrated that the Alum Fork area revealed many characteristics of sheath folds described elsewhere (e.g. Borradaile 1972, Ramsay 1979). Viele & Reader (1985) argued that sheath folds are common across most of the Benton uplift. Sheath folds generated as the result of progressive simple shear have been documented both in the field and the laboratory (Borradaile 1972, Ramsay 1979, Cobbold & Quinquis 1980, Lacassin & Mattauer 1985, among others). Evidence for simple shear in Benton uplift include extreme attenuation and faulting on regional fold limbs, and rotated pyrite grains (Sturges 1986).

Traditionally, determination of shear strain in deformed rocks depends on the presence of suitable strain markers. Unfortunately, such strain markers are lacking in the Broken Bow uplift except for the deformed pebbles found near the DMFZ. Lacassin & Mattauer (1985) studied a kilometer-scale sheath fold at Mattmark in the Alps. They concluded that hinge lines of the sheath fold had been passively rotated as a result of simple shear. By assuming a simple-shear model, Lacassin & Mattauer (1985) were able to calculate the shear strain associated with those rotations. They proposed that such an estimate of shear strain would be more significant than the commonly used center to center strain techniques (Fry 1979) because it would represent the average bulk shear strain for the whole volume of rock.

Alsop (1992) modified this geometrical model to calculate bulk shear strain from rotated fold-hinge lines in the Ballybofey Nappe, northwest Ireland. Alsop's model assumed that the original fold-hinge lines ( $xy$ ) lie in a plane that is perpendicular to the shear direction (Fig. 13a). As a result of progressive simple shear, original fold hinge lines are rotated to  $x'y'$ . In this model,  $B/C$  describes the initial obliquity between fold-hinge lines and the shear direction and  $\alpha'$  is the angle between rotated fold-hinge lines ( $x'y'$ ) and the transport direction, which is 'mineral lineation' (Fig. 13a). Minor folds oriented at angles of  $70^{\circ}$ – $80^{\circ}$  from mineral lineation are subsequently rotated towards the shear direction. Clearly  $B/C$  only gives the angle between initial fold-hinge lines and the shear plane in the plane perpendicular to shear direction instead of the initial obliquity between fold-hinge lines and shear direction. In Alsop's model the angle between initial fold-hinge lines and shear direction is always  $90^{\circ}$ . The plane containing  $X'Y'$  in Alsop's model (Fig. 13a) is neither the shear plane nor the flattening plane. Therefore,  $\alpha'$  does not represent

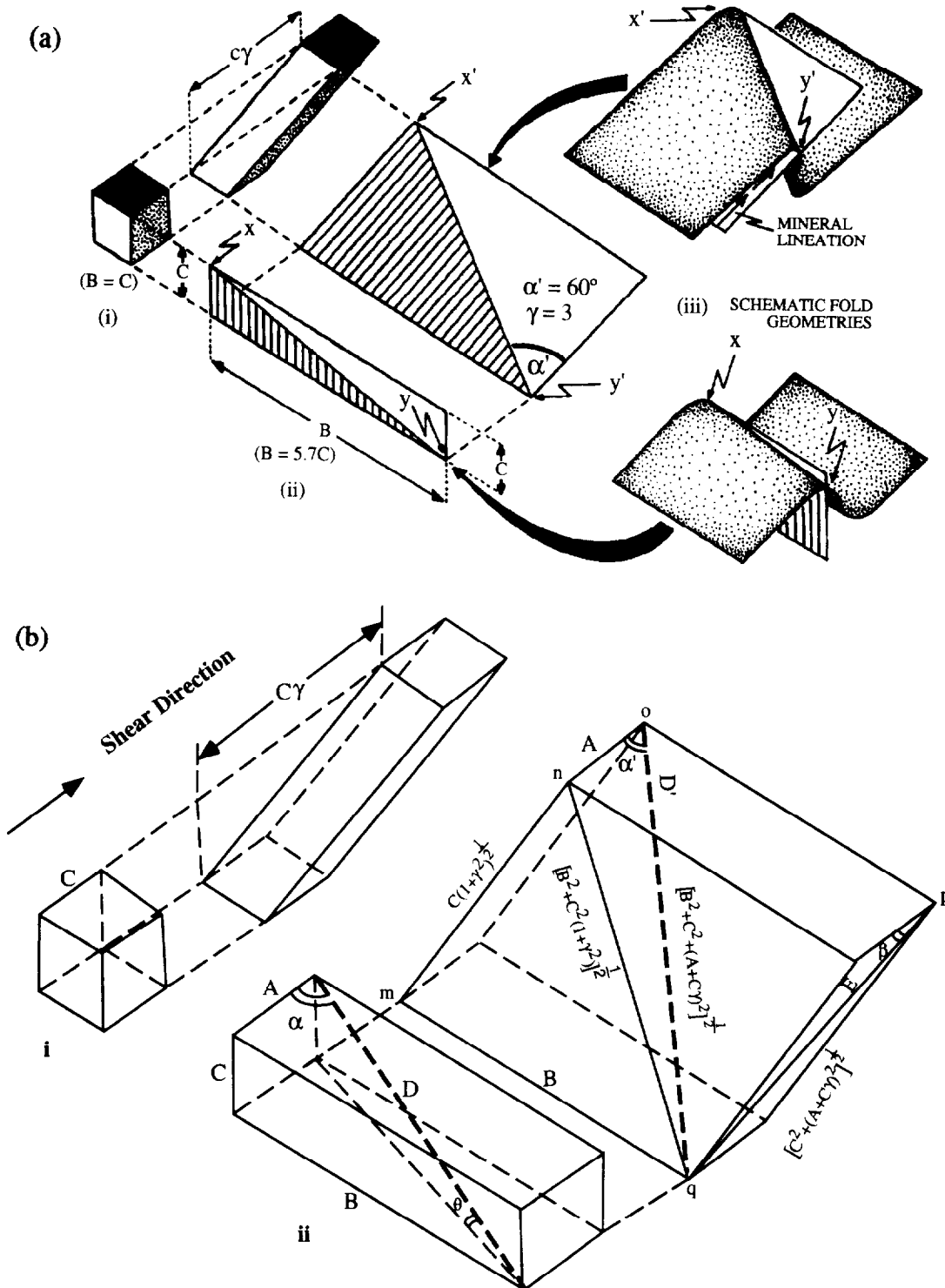


Fig. 13. (a) Progressive rotation of fold-hinge lines (after Alsop 1992). (i) Idealized simple shear deformation of a cube (side  $C$ ) and shear strain  $\gamma$ . (ii) The same deformation applied to a cross-section ( $B-C$ ) representing obliquely oriented fold-hinge lines.  $\alpha'$  represents the acute angle between fold-hinge lines and the transport direction, which is a function of  $\gamma$  and the initial fold orientation ( $B-C$ ). (iii) Schematic fold geometry pertaining to (ii). (b) Progressive reorientation of fold-hinge lines by simple shear (modified from Alsop 1992). (i) Idealized deformation of a cube with side equal to  $C$  and shear strain  $\gamma$ . (ii) The same deformation applied to a cube with edge  $A$  parallel to shear direction.

the angle either between rotated fold-hinge lines and the shear direction or between rotated fold-hinge lines and extension direction although these angles will be close to each other at high strain.

Alsop's model is only suitable for a special case. A more generally applicable model is proposed (Fig. 13b). Assuming that fold-hinge lines are passively rotated due

to progressive simple shear and that initial angles between the shear direction and fold-hinge lines are known, shear strain ( $\gamma$ ) can be calculated using the following geometric relationship (see Appendix):

$$\gamma = \frac{\cot(\alpha') * \sqrt{B^2 + C^2 - A}}{C}$$

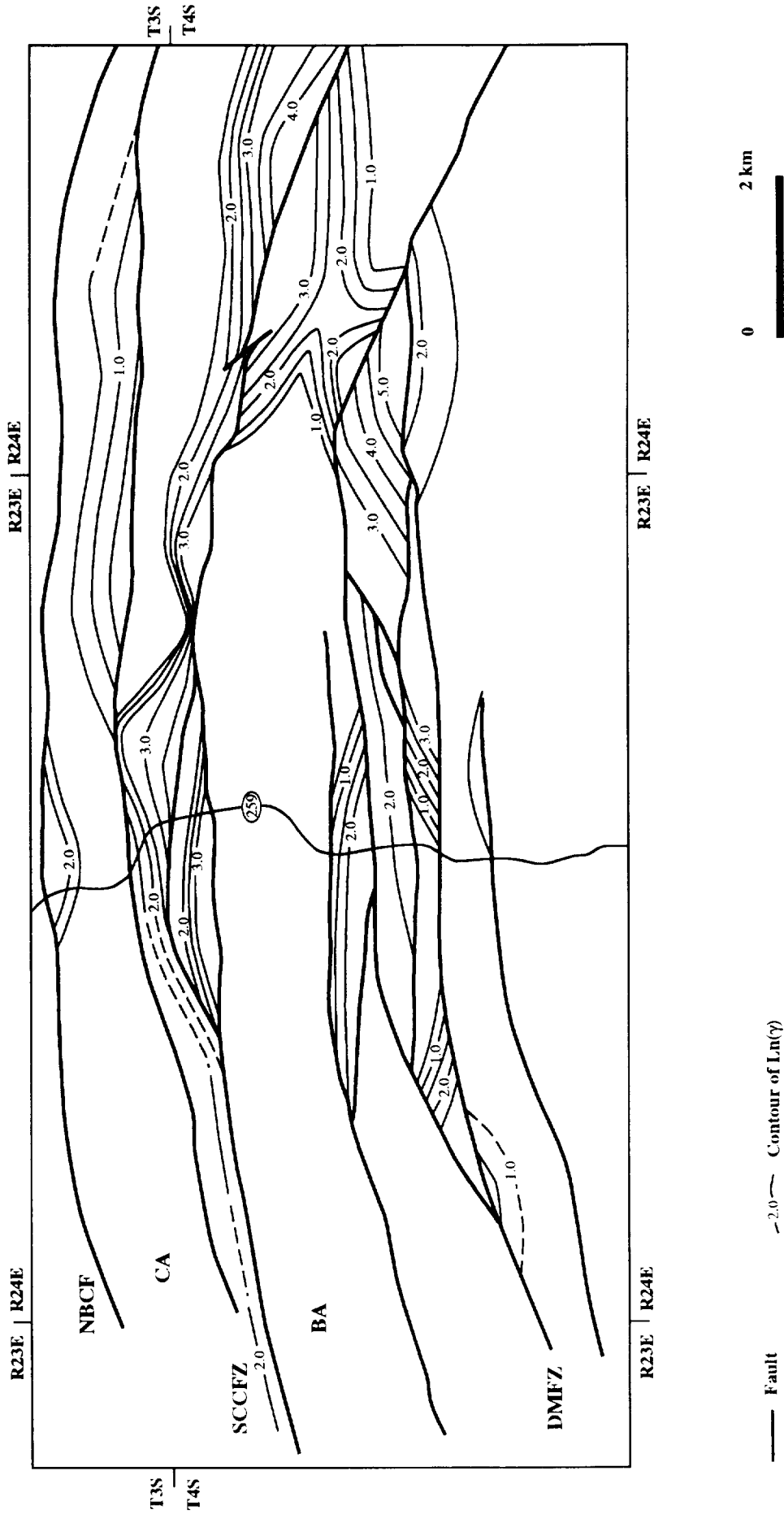


Fig. 14. Map showing distribution of shear strain in the study area.

$$= \frac{\cot(\alpha') * \sin(\alpha) - \cos(\alpha)}{\sin(\theta)} \quad (1)$$

In this model,  $\alpha$  is the angle between initial fold-hinge lines ( $D$ ) and the shear direction ( $A$ ).  $\alpha'$  is the angle between rotated fold-hinge lines and the shear direction.  $\theta$  represents the angle between initial fold-hinge lines and the shear plane. The lengths of  $A$ ,  $B$  and  $C$  depend on the angles  $\alpha$  and  $\theta$ . By equation (1), shear strain can be estimated if the initial orientation of fold-hinge lines, the shear direction and the shear plane are known or can be estimated.

The geometry of the earliest fold has been documented throughout the Broken Bow uplift (Feenstra & Wickham 1975, Nielsen *et al.* 1989, Yang & Nielsen 1992a). We assume that orientation of folds in the footwall of the DMFZ represents initial folds because these folds are least affected by simple shear associated with the fault zones. Sanderson (1973) suggested that the variation of fold-hinge-line orientation is commonly up to 25°. We believe that the initial fold-hinge lines in this portion of Broken Bow uplift vary much less. All the earliest folds documented generally trend E–W and are subhorizontal (Figs. 5, 6 and 7).

As discussed earlier, fold-hinge lines within the fault zones have been significantly rotated (Fig. 9). If all the fold-hinge lines within the fault zones have been rotated towards the shear direction, the best fit circle defined by the fold-hinge lines (Fig. 12) outlines a plane that approaches the attitude of the shear plane at high shear strain.

At high shear strain, the shear direction approximates extension direction. Thus, the shear direction is approximated by the deformed clasts along the DMFZ, since no other strain markers have been found in the study area. We would like to emphasize that the shear direction may vary locally or from region to region. The extensional lineations documented in the Monte Rosa nappe, Swiss Alps by Lacassin & Mattauer (1985) indicate 70° (N70°E to N140°E) variation. Our data also show variation of about 80° (N80°W to N). Thus, the shear strain calculation is only an approximation and represents an average shear strain for the whole volume of rock.

Based on these assumptions, the shear strain associated with each rotated fold-hinge lines can be calculated. The large variation of shear strain ( $0 < \gamma < 180^\circ$ ) across the study area makes it difficult to analyze and contour. Therefore,  $\ln \gamma$  has been calculated, plotted, and contoured on the map where only fault traces are shown (Fig. 14). The strain pattern has the following characteristics. Shear strain is mainly concentrated in the fault zones. There seems to be no shear strain associated with the footwall of the DMFZ, the Carter Mountain anticline, or Brigham anticline, which are interpreted to be associated with the earliest folds. As the fault zones are approached from either the footwall or hangingwall, a small amount of shear strain is recorded. However, high shear strains are also indicated in the eastern end of Brigham anticline in the proximity of the DMFZ and SCCFZ. Our current interpretation is that the variation

indicates possible fault splays and small horse blocks developed in this area.

In general  $\gamma$  values are around 20 ( $\ln \gamma = 3$ ) within the fault zones although strain values as high as 180 ( $\ln \gamma = 5$ ) are indicated locally. Within the SCCFZ the shear strain increases from north to south. The  $\ln \gamma$  values are usually around 2 in the north and 3 to 4 in the south. Within individual horse blocks of the DMFZ, shear strain also increases from north to south. The other characteristic of the DMFZ is an increase of shear strain as the tip of horse blocks are approached. The pattern of shear strain reflects inhomogeneous deformation within the fault zones. As the fault planes are approached, shear strain increases significantly. However, this variation may partly be related to the tangent function. A small change of  $\alpha$  value can significantly change the value of  $\gamma$  when  $\alpha$  is small. That is to say, where the fold-hinge lines are rotated nearly parallel to the shear direction, the relationship is less sensitive.

## DISCUSSION

This model assumes constant volume deformation. Cleavage development in the footwall of the DMFZ is attributed to the earliest deformation and rotated by second generation folding. Microfold morphology indicates that at least 30% volume loss during cleavage formation due to pressure solution (Yang & Nielsen 1992b). In addition to the slaty cleavage, a rough cleavage is associated with third generation structures (Shore & Nielsen 1987). This N-dipping rough cleavage is usually located on the S-dipping limbs of second generation synforms and believed to be related to the flattening. No similar cleavage has been documented within the fault zones. It is assumed that no significant volume loss is associated with the fault zone development. If there is, then the shear strain has been over estimated.

Our studies indicate that only fold-hinge lines within the fault zones have been significantly rotated during S-directed thrusting. Therefore, by calculating and contouring the shear strain associated with each rotated fold-hinge line, fault zones may be mapped in area of poor exposure.

Due to lack of any other strain markers, the best fit great circle to hinge lines (Fig. 12) is used to approximate the shear plane. The shear plane is separated from the best fit great circle by the angle ( $\beta$ ) which is equivalent to  $\arctan [1/(\gamma + \cos \alpha / \sin \theta)]$  or in this specific case  $\arctan 1/(\gamma + 12.6)$  (Fig. 13b). Thus, the calculated shear strain will be overestimated. In a high-shear-strain regime,  $\beta$  becomes very small. In the Broken Bow uplift,  $\beta$  is around 3° at  $\gamma$  values of 5 and as small as less than 2° at  $\gamma$  values of 20. Our ability to refine the orientation of fault zones is limited by the poor exposure.

Initial geological mapping of the Broken Bow uplift by Honess (1923, p. 216) led him to believe that deformation observed in rocks overlying the Womble Formation represent 'a shrinkage or shortening of the

earth's crust in this region of several miles'. Miser (1929) mapped the Potato Hills, which are located approximately 50 km northwest of the Broken Bow uplift. He stated that the Windingstair fault had been folded and rocks of Ordovician, Silurian and Devonian age have been thrust northward over the Stanley Shale along the Windingstar fault. Similarly, based on Honess' mapping, Miser (1929) interpreted that the flank sequence in the Broken Bow uplift is detached from the core of the uplift. Pitt (1955) remapped the central core of the Broken Bow uplift and concluded that the sequence is autochthonous and forms a large anticlinorium rather than part of a thrust sheet. Misch & Oles (1957) agreed with Pitt and said that the Ouachita Mountains are an autochthonous folded system rather than an overthrust. Based on the calculated shear strain values presented in this paper, it is clear that large shear strains are associated with the S-directed thrusting in the Broken Bow uplift. As Lacassin & Mattauer (1985) pointed out, these  $\gamma$  values suggest significant amount of displacement. For a fault zone of 0.3–1 km thick in the study area, the displacement may range from 6 km to 20 km. Thus the Carter Mountain anticlinorium is allochthonous relative to Hochatown dome and tens of kilometers of translation are indicated.

### CONCLUSIONS

(1) Compared with Alsop's model, our geometric model is more generally applicable and can be used to calculate shear strain from rotated fold-hinge lines.

(2) The shear strain calculated from passively rotated fold-hinge lines provides an estimate of the incremental strain associated with shear-zone development. Therefore, this improved method provides an approach for studying strain factorization associated with progressive deformation in Ouachita Mountains as well as other orogenic belts.

(3) The study indicates that the Carter Mountain anticlinorium north of the DMFZ is allochthonous relative to the Hochatown dome and has been translated southwards for tens of kilometers.

*Acknowledgements*—We would like to thank Karl Fleischmann, Kristain Soegaard and Bob Stern for constructive discussions and reviews of this manuscript. Thanks are also due to J. W. Handschy, J. Mies and S. F. Wojtal for their thorough reviews and helpful criticisms which significantly improved the manuscript.

### REFERENCES

- Alsop, G. I. 1992. Progressive deformation and the rotation of contemporary fold axes in the Ballybofey Nappe, north-west Ireland. *Geol. J.* **27**, 271–283.
- Arbenz, J. K. 1989. Ouachita thrust belt and Arkoma basin. In: *The Appalachian–Ouachita Orogen in the United States, The Geology of North America* (edited by Hatcher, R. D. Jr., Thomas W. A. & Viele, G. W.). **F-2**, 621–634.
- Bell, T. H. 1978. Progressive deformation and reorientation of fold axes in a ductile mylonite zone, the Woodroffe thrust. *Tectonophysics* **44**, 285–321.
- Borradaile, G. J. 1972. Variable oriented co-planar primary folds. *Geol. Mag.* **109**, 89–98.
- Bryant, B. & Reed, J. C. 1969. Significance of lineation and minor folds near major thrust faults in the southern Appalachian and the British and Norwegian Caledonides. *Geol. Mag.* **106**, 412–429.
- Cobbold, P. & Quinquis, H. 1980. Development of sheath fold in shear regimes. *J. Struct. Geol.* **2**, 119–126.
- Cowan, D. S. & Brandon, M. T. 1994. A symmetry-based method for kinematic analysis of large-slip brittle fault zones. *Am. J. Sci.* **294**, 257–306.
- Coward, M. P. & Potts, G. J. 1983. Complex strain patterns developed at the frontal and lateral tips to shear zones and thrust zones. *J. Struct. Geol.* **5**, 383–399.
- Denison, R. E., Burke, W. H., Otto, J. B. & Heatherington, E. A., Jr. 1977. Age of igneous and metamorphic activity affecting the Ouachita foldbelt. In: *Symposium on the Geology of the Ouachita Mountain* (edited by Stone, C. G.). *Arkansas Geological Commission* **1**, 25–40.
- Denison, R. E., Kenny, G. S., Burke, W. H., Jr. & Heatherington, E. A., Jr. 1969. Isotopic ages of igneous and metamorphic boulders from the Haymond Formation (Pennsylvanian), Marathon Basin, Texas, and their significance. *Bull. geol. Soc. Am.* **80**, 245–256.
- Escher, A. & Watterson, J. 1974. Stretching fabrics, folds and crustal shortening. *Tectonophysics* **22**, 223–231.
- Feenstra, R. & Wickham, J. 1975. Evolution of folds around Broken Bow uplift, Ouachita Mountains, southeastern Oklahoma. *Bull. Am. Ass. Petrol. Geol.* **59**, 975–985.
- Flawn, P. T., Goldstein, A., King, P. B. & Weaver, C. E. 1961. The Ouachita System. The University of Texas Bureau of Economic Geology Publication 6120, Austin, Texas.
- Flinn, D. 1962. On folding during three-dimensional progressive deformation. *J. geol. Soc. Lond.* **118**, 385–433.
- Fry, N. 1979. Density distribution techniques and strained length methods for determination of finite strains. *J. Struct. Geol.* **1**, 221–229.
- Ham, W. E. & Wilson, J. E. 1967. Paleozoic epirogeny and orogeny in the central U.S. *Am. J. Sci.* **265**, 332–407.
- Handschy, J. W. 1989. Sedimentology and Structural Geology of the Endicott Mountains Allochthon, central Brooks Range, Alaska. Unpublished Ph.D. dissertation, Rice University.
- Herrin, E. & Clark, S. P., Jr. 1956. Heat flow in west Texas and eastern New Mexico. *Geophysics* **21**, 1087–1089.
- Honess, C. W. 1923. Geology of Southern Ouachita Mountains of Oklahoma. *Bull. geol. Surv. Oklahoma* **32**, part 1.
- Houseknecht, D. W. & Matthews, S. M. 1985. Thermal maturity of Carboniferous strata, Ouachita Mountains. *Bull. Am. Ass. Petrol. Geol.* **69**, 335–345.
- Keller, W. D., Stone, C. G. & Hoersch, A. L. 1985. Textures of Paleozoic chert and novaculite in the Ouachita Mountains of Arkansas and Oklahoma and their geological significance. *Bull. geol. Soc. Am.* **96**, 1353–1363.
- Lacassin, R. & Mattauer, M. 1985. Kilometre-scale sheath fold at Mattmark and implications for transport direction in the Alps. *Nature* **315**, 739–742.
- Lisle, R. J. 1985. *Geological Strain Analysis: A Manual for the R<sub>1</sub>/φ Technique*. Pergamon Press, Oxford.
- Mattes, J. & Nielsen, K. C. 1983. Age relationships of structures along the western flank of the Broken Bow uplift. *Geol. Soc. Am. Abstr. w. Prog.* **15**, 1.
- Mickus, K. L. & Keller, G. R. 1992. Lithospheric structure of the south-central United States. *Geology* **20**, 335–338.
- Mies, J. W. 1991. Planar dispersion of folds in ductile shear zones and kinematic interpretation of fold-hinge girdles. *J. Struct. Geol.* **13**, 281–297.
- Minnigh, L. D. 1979. Structural analysis of sheath folds in meta-chert from the western Italian Alps. *J. Struct. Geol.* **1**, 275–282.
- Miser, H. D. 1929. Structure of the Ouachita Mountains of Oklahoma and Arkansas. *Bull. geol. Surv. Oklahoma* **50**.
- Misch, P. & Oles, K. F. 1957. Interpretation of the Ouachita Mountains of Oklahoma as autochthonous folded belt. *Bull. Am. Ass. Petrol. Geol.* **41**, 1899–1905.
- Nielsen, K. C. 1985. Integrated structural model for the Broken Bow uplift, southeastern Oklahoma. *Geol. Soc. Am. Abstr. w. Prog.* **17**, 186.
- Nielsen, K. C., Viele, G. W. & Zimmerman, J. 1989. Structural setting of the Benton–Broken Bow uplifts. In: *The Appalachian–Ouachita Orogen in the United States, The Geology of North Amer-*

- ica (edited by Hatcher, R. D., Jr., Thomas, W. A. & Viele, G. W.). **F-2**, 635–660.
- Nielsen, K. C. & Yang, Q. 1992. Southerly vergence associated with northerly directed thrusts of Ouachita Mountains of Oklahoma. *Geol. Soc. Am. Abstr. w. Prog.* **24**, 41.
- Nielsen, K. C. & Yang, Q. In press. The Dyer Mountain fault zone, southerly directed thrusts, Broken Bow Uplift. *Spec. Publ. Oklahoma Geol. Surv.*
- Pitt, W. D. 1955. Geology of the core of the Ouachita Mountains in Oklahoma. *Oklahoma Geol. Surv. Circ.* **34**.
- Quinquis, H., Audren, C., Brun, J. P. & Cobbold, P. R. 1978. Intense progressive shear in Ile de Groix blueschists and compatibility with subduction or obduction. *Nature* **273**, 43–45.
- Ramsay, D. M. 1979. Analysis of rotation of folds during progressive deformation. *Bull. geol. Soc. Am.* **90**, 732–738.
- Rhodes, S. & Gayer, R. A. 1977. Non-cylindrical folds, linear structures in the X-direction and mylonite developed during translation of the Caledonian Kalak Nappe Complex of Finnmark. *Geol. Mag.* **114**, 329–341.
- Ridley, J. 1986. Parallel stretching lineations and fold axes oblique to a shear displacement direction—a model and observations. *J. Struct. Geol.* **8**, 647–653.
- Roberts, J. L. & Sanderson, D. J. 1973. Oblique fold axes in the Dalradian rocks of the southwest Highlands. *Scott. J. Geol.* **9**, 281–296.
- Sanderson, D. J. 1973. The development of fold axes oblique to the regional trend. *Tectonophysics* **16**, 55–70.
- Shore, P. S. & Nielsen, K. C. 1987. Pencil lineations and coaxial deformation, Broken Bow uplift, southeastern Oklahoma. *Geol. Soc. Am. Abstr. w. Prog.* **19**, 843.
- Sturgess, S. 1986. Structural geology of the Alum Fork area, Benton uplift, Arkansas. Unpublished M.S. thesis, The University of Missouri, Columbia, U.S.A.
- Viele, G. W. 1989. The Ouachita orogenic belt. In: *The Appalachian–Ouachita Orogen in the United States, The Geology of North America* (edited by Hatcher, R. D., Jr., Thomas, W. A. & Viele, G. W.). **F-2**, 555–562.
- Viele, G. W. & Reader, J. M. 1985. Geometry of 2nd phase folding, Benton uplift, Arkansas. *Geol. Soc. Am. Abstr. w. Prog.* **17**, 196.
- Viele, G. W. & Thomas, W. A. 1989. Tectonic synthesis of the Ouachita orogenic belt. In: *The Appalachian–Ouachita Orogen in the United States, The Geology of North America* (edited by Hatcher, R. D., Jr., Thomas, W. A. & Viele, G. W.). **F-2**, 696–728.
- Williams, G. D. 1978. Rotation of contemporary folds into X-direction during overthrust processes in Laksefjord, Finnmark. *Tectonophysics* **48**, 29–40.
- Wojtal, S. 1986. Deformation within foreland thrust sheets by populations of minor faults. *J. Struct. Geol.* **8**, 341–360.
- Yang, Q. & Nielsen, K. C. 1992a. The Dyer Mountain fault zone, Broken Bow uplift, southeastern Oklahoma. *Geol. Soc. Am. Abstr. w. Prog.* **24**, 51–52.
- Yang, Q. & Nielsen, K. C. 1992b. Progressive deformation of slaty cleavage in the Broken Bow Uplift, Oklahoma. *Geol. Soc. Am. Abstr. w. Prog.* **24**, 183.
- Yang, Q. 1993. Deformation of the Broken Bow uplift, Ouachita Mountains, Southeastern Oklahoma. Unpublished Ph.D. dissertation, University of Texas at Dallas.
- Yang, Q. & Nielsen, Kent C. 1993. Rotation of fold axes during southerly directed thrusting, Broken Bow uplift, Ouachita Mountains of Oklahoma. *Geol. Soc. Am. Abstr. w. Prog.* **25**, 46–47.

## APPENDIX

To find the shear strain associated with rotated fold-hinge lines, one simply applies a simple shear strain of  $\gamma$  so that an original cube will be deformed into rhombohedron. The shear strain can be determined based on the general geometrical relationships among the initial fold hinge lines, rotated fold hinge lines, shear plane, and shear direction. The following lists the main steps for the derivation (also see Fig. 13b)

$$mn = \sqrt{C^2 + C^2\gamma^2} = C\sqrt{1 + \gamma^2} \quad (\text{A1})$$

$$nq = \sqrt{mq^2 + mn^2} = \sqrt{B^2 + C^2 * (1 + \gamma^2)} \quad (\text{A2})$$

$$pq = \sqrt{C^2 + (C\gamma + A)^2} \quad (\text{A3})$$

$$oq = \sqrt{op^2 + pq^2} = \sqrt{B^2 + C^2 + (C\gamma + A)^2}. \quad (\text{A4})$$

For triangle  $noqn$ , the law of cosine gives

$$nq^2 = no^2 + oq^2 - 2 * no * oq * \cos(\alpha'). \quad (\text{A5})$$

Substituting using equations (A1)–(A4) yields

$$B^2 + C^2(1 + \gamma^2) = A^2 + B^2 + C^2 + (C\gamma + A)^2 - 2 * A * \sqrt{B^2 + C^2 + (C\gamma + A)^2} * \cos(\alpha'). \quad (\text{A6})$$

Rearrange the above equation to get

$$A + C\gamma = \sqrt{B^2 + C^2 + (A + C\gamma)^2} * \cos(\alpha'). \quad (\text{A7})$$

Then

$$\gamma = \frac{(\tan(\alpha'))^{-1} * \sqrt{B^2 + C^2} - A}{C} \quad (\text{A8})$$

or

$$\gamma = \frac{\cot(\alpha') * \sqrt{B^2 + C^2} - A}{C}. \quad (\text{A9})$$

Since

$$C = D * \sin(\theta), \quad A = D * \cos(\alpha),$$

and

$$B = D * \sqrt{(\cos^2(\theta) - \cos^2(\alpha))} \\ \gamma = \frac{(\cot(\alpha'))\sqrt{\cos^2(\theta) - \cos^2(\alpha)} + \sin^2(\theta) - \cos(\alpha)}{\sin(\theta)}. \quad (\text{A10})$$

Substituting  $\sin^2(\theta) + \cos^2(\theta) = 1$  and  $1 - \cos^2(\alpha) = \sin^2(\alpha)$  yields

$$\gamma = \frac{\cot(\alpha') * \sin(\alpha) - \cos(\alpha)}{\sin(\theta)}. \quad (\text{A11})$$